Journal of Nano- and Electronic Physics
Vol. **18** No 5, 05033(9pp) (2026)

Журнал нано- та електронної фізики
Том **18** № 5, 05033(9cc) (2026)

OPEN ACCESS

REGULAR ARTICLE

Application-Specific Thickness Optimization for Organic Solar Cells Under Indoor and Outdoor Conditions

W. Guanoune[1,*], H.A. Abbassi[2]

[1] *Badji Mokhtar University, Faculty of Sciences, Department of Physics, 23000 Annaba, Algeria*
[2] *Environmental Research Center (CRE), Environmental Innovation and Eco-Waste Management Division, 23000 Annaba, Algeria*

(Received 15 July 2026; revised manuscript received 19 October 2026; published online 28 October 2026)

Organic solar cells (OSCs) offer flexibility and low-cost fabrication, but their performance is strongly dependent on illumination conditions. Standard optimization under AM1.5G (1000 W·m^{-2}) does not reflect the diversity of real environments, which range from sub-watt indoor light to full sunlight. In this work, we establish illumination-dependent thickness guidelines that link device geometry to targeted applications. Drift–diffusion simulations using OghmaNano (GPVDM) were performed on bulk-heterojunction P3HT:PCBM solar cells across intensities from 0.5 to 1100 W·m^{-2}. The results show that under indoor conditions (1-30 W·m^{-2}), thicker active layers (350-400 nm) maximize absorption and yield power conversion efficiencies (PCE) up to 3.75 %, whereas under high outdoor irradiance (≥ 700 W·m^{-2}), thinner layers (200-230 nm) mitigate recombination and enhance energy output. A design map relating PCE, *J*sc, *V*oc, and *FF* to thickness–intensity pairs identifies application-specific optima. Although demonstrated on P3HT:PCBM as a reference system, the methodology is broadly applicable to other organic photovoltaic technologies. These results provide concise, illumination-aware thickness guidelines that bridge laboratory optimization with real-world deployment of OSCs under indoor and outdoor conditions.

Keywords: Organic solar cells, Active-layer thickness, Drift-diffusion simulation, Light-intensity dependence, Indoor photovoltaics.

DOI: 10.21272/jnep.18(5).05033 PACS numbers: 84.60.Jt, 72.80.Le, 73.61.Ph

1. INTRODUCTION

The transition to low-carbon energy requires a rapid increase in renewable electricity. In 2022, renewable sources produced almost 30 % of the world's electricity, and this share is expected to rise further with policies following the Paris Agreement [1]. Photovoltaics (PV) is a central technology in this process because it can be deployed at different scales. Yet crystalline silicon, which dominates the PV market, has well-known limitations: its production is energy-intensive, the material is rigid, and it is not ideal for lightweight or flexible devices [2, 3].

Organic solar cells (OSCs) have been studied for more than twenty years as an alternative. They can be processed from solution, are mechanically flexible, and their absorption can be tuned. These features make them attractive for applications such as wearable devices, integrated sensors, or indoor photovoltaics [4]. Still, their efficiency and long-term stability remain below those of inorganic technologies [5, 6]. On the other hand, their compatibility with low-cost printing and roll-to-roll fabrication methods provides them an edge for specific, low-power applications. At the microscopic level, the bulk heterojunction (BHJ) structure, where donor and acceptor phases form an interpenetrating network, remains the most effective design for exciton separation and charge transport [7].

Currently, crystalline silicon represents about 98 % of the PV market, while thin-film technologies such as CdTe, CIGS, and a-Si account for roughly 2 %. OSCs make up less than 0.1 % of production, but their projected growth (23 % CAGR) [8, 9] maintains strong interest in their physics and device optimization. With the development of non-fullerene acceptors (NFAs) and tandem structures, the efficiency of single-junction OSCs has reached 19-20 % [10, 11], and tandem devices have already exceeded 20 % [12, 13]. These results show the importance of nanoscale morphology and charge transport in improving performance.

External conditions, especially illumination. Standard testing under AM1.5G (1000 W·m^{-2}) does not reflect the wide range of real operating environments, from weak indoor lighting to full outdoor sunlight [14, 15]. Figure 1 illustrates the variations in global horizontal irradiation (GHI), which differ considerably across geographical regions [16]. Such diversity underlines the need to design OSC architectures with the illumination context in mind.

* Correspondence e-mail: guanoune.walid@gmail.com

© 2026 The Author(s). Journal of Nano- and Electronic Physics published by Sumy State University. This article is distributed under the terms and conditions of the Creative Commons Attribution (CC BY) license.

Cite this article as: W. Guanoune, et al., *J. Nano- Electron. Phys.* 18 No 5, 05033 (2026) https://doi.org/10.21272/jnep.18(5).05033

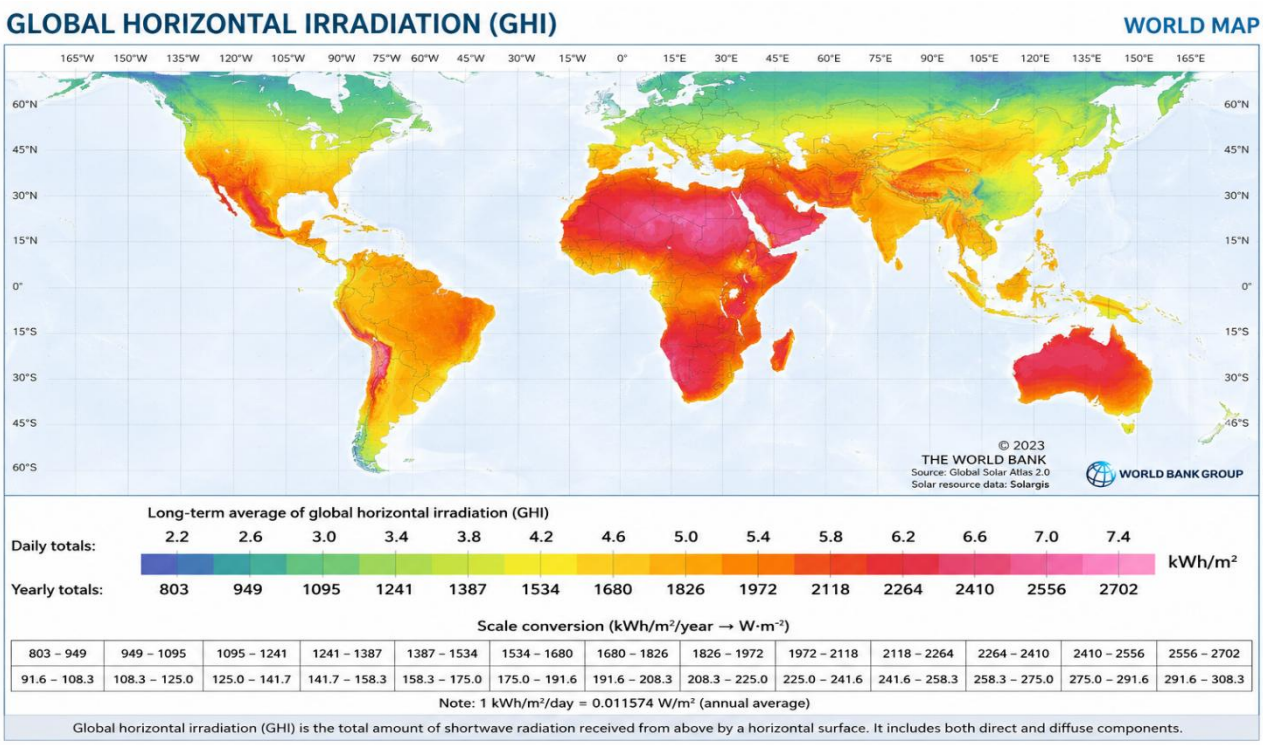


Fig. 1 – Annual mean global horizontal irradiance (GHI) in W·m^{-2}. Adapted from the Global Solar Atlas 2.12 [16]

The thickness of the active layer plays a crucial role, as it governs the balance between optical absorption and charge transport. Many studies have examined either the influence of thickness or the impact of illumination, but only a limited number have considered both aspects together within an application-oriented framework [17, 18].

In this work, we explore how active-layer thickness and illumination level interact in bulk heterojunction (BHJ) OSCs using the OghmaNano (GPVDM) simulation platform. P3HT:PCBM is chosen as a model system because its morphology and electronic parameters are well documented, making it a reliable benchmark for reproducible simulations [19, 20]. At the same time, the approach presented here is not confined to this blend: the illumination-aware optimization framework can be readily extended to modern OSCs, including NFA-based blends, ternary systems, and tandem devices.

By systematically analyzing the dependence of *J*sc, *V*oc, *FF*, and PCE on thickness–intensity combinations across the range of 0.5-1100 W·m^{-2}, we identify conditions that yield application-specific optima for both indoor and outdoor operation. This study therefore provides practical guidelines for device design and establishes a generalizable framework that connects nanoscale optimization with real-world deployment of organic solar cells.

2. METHODOLOGY AND DEVICE ARCHITECTURE

2.1 Simulation Tool and Integrated Physical Model

In this work, the simulations were carried out with GPVDM (General Purpose Photovoltaic Device Model). This program is a multiphysics tool that can handle different optoelectronic devices: inorganic, organic, and perovskite solar cells [21]. It is also used for LEDs, photodetectors, and thin-film transistors.

The core of the solver is based on drift-diffusion and Poisson equations, coupled with a non-equilibrium Shockley-Read-Hall (SRH) model. With this combination, the program can reproduce charge generation, transport, and recombination. This is particularly useful in the case of disordered organic semiconductors, where traps strongly affect transport and recombination.

Charge transport is governed by the drift–diffusion equations:

$$J_n = q\mu_e n_f \frac{\partial E_{LUMO}}{\partial x} + qD_n \frac{\partial n_f}{\partial x} \quad (1)$$

$$J_p = q\mu_p p_f \frac{\partial E_{HOMO}}{\partial x} + qD_p \frac{\partial p_f}{\partial x} \quad (2)$$

where J_n and J_p denote the current densities of electrons and holes, respectively; q is the elementary charge; μ_n and μ_p are the corresponding carrier mobilities; n_f and p_f represent the free carrier densities; E_{LUMO} and E_{HOMO} refer to the LUMO and HOMO energy levels; and D_n and D_p are the diffusion coefficients of electrons and holes, respectively.

Charge conservation is expressed by the continuity equations:

$$\frac{\partial J_n}{\partial x} = q(R - G) \quad (3)$$

$$\frac{\partial J_p}{\partial x} = -q(R - G) \quad (4)$$

where R and G denote the recombination and generation rates of charge carriers, respectively.

The electrostatic potential is obtained from Poisson's equation:

$$\frac{d}{dx}\epsilon_0\epsilon_r\frac{d\Phi}{dx} = q(n_f + n_t - p_f - p_t - N_{ad}) \quad (5)$$

where ε_0 is the vacuum permittivity, ε_r is the relative permittivity of the active medium, Φ is the electrostatic potential, n_t and p_t denote the trapped electron and hole densities, and N_{ad} is the density of ionized dopants.

Carrier mobilities follow a trap-limited dependence:

$$\mu(n) = \mu_0 \cdot \frac{n_{free}}{n_{free}+n_{trapped}} \quad (6)$$

where μ_0 is the intrinsic mobility, n_{free} is the density of free carriers, and n_{trapped} is the density of trapped carriers.

In practice, the density of states (DOS) is described with an exponential tail, divided into 160 discrete energy levels. Each level is linked to a quasi-Fermi level, which lets the simulation capture trapping and detrapping events, charge build-up, and transient behavior.

Two recombination channels are included:

– Langevin-type bimolecular recombination.

– Trap-assisted recombination, which dominates in disordered OSCs and is described by the SRH model.

Figure 2 shows how trap occupation depends on both energy and spatial position under illumination and stresses the role of traps near the donor–acceptor interface.

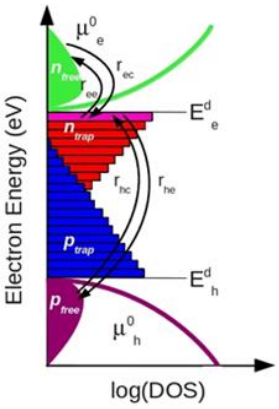


Fig. 2 – Illustrates the evolution of trap occupancy as a function of both energy and spatial position within the device under illumination [22]

2.2 Reference Active Layer System

The active layer studied here is the classic donor-acceptor blend P3HT:PCBM. This system was picked for several reasons.

1. **Well-known properties.** P3HT:PCBM has been tested in many labs, both experimentally and theoretically. Its main parameters, such as mobility, absorption, energy levels, and trap states, are well reported and usually reproducible. For that reason, it is a solid base for modeling. Experimental studies have investigated how molecular weight and regioregularity affect the performance of P3HT:PCBM devices [23], how traps influence charge transport and recombination [24], how thickness changes parameters [25], and how to extract them from J–V curves [26].
2. **Morphological stability.** This blend makes stable bulk-heterojunction (BHJ) films that can be processed in air without special encapsulation. That is useful for fundamental work, for flexible devices, and for large-area fabrication. Reports show that P3HT:PCBM layers keep their morphology even when made under normal lab conditions [27], so they stay a reliable reference for OSC studies [28].
3. **Accessibility.** P3HT and PCBM are commercially available and compatible with relatively simple solution-processing techniques, which has contributed to the widespread use of P3HT:PCBM as a model system in organic photovoltaic research [29, 30].
4. **Benchmark role.** As one of the most studied blends, P3HT:PCBM is a natural baseline for simulations. Using it avoids the uncertainty that comes with newer materials and makes comparisons between different architectures more consistent [31].

It becomes easier to highlight the proposed method of illumination-aware thickness optimization using this established system, free from material-specific uncertainties.

2.3 Simulated Device Structure

The simulated solar cell is based on a conventional bulk-heterojunction (BHJ) design. In this structure, the donor and acceptor phases form a nanoscale, interpenetrating network.

Figure 3 presents an overview of the system. Panel (a) presents the full device stack: ITO as the anode, a PEDOT:PSS hole transport layer, the P3HT:PCBM active layer, and finally an aluminum cathode. Panel (b) shows the morphology of the P3HT:PCBM blend, where the mixed donor and acceptor domains create pathways that allow excitons to dissociate and charges to move.

Table 1 – Layer structure of the simulated P3HT:PCBM solar cell

Layer	Material	Thickness (nm)
Anode	Indium Tin Oxide (ITO)	100
Hole Transport Layer	PEDOT:PSS	100
Active Layer	P3HT:PCBM blend	100-400 (variable)
Cathode	Aluminum	100

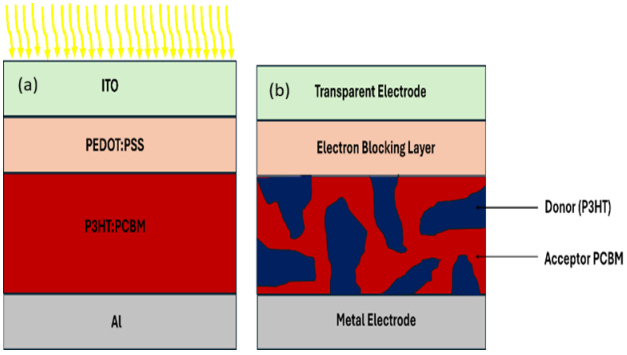


Fig. 3 – (a) Layer structure of the simulated device: ITO/PEDOT:PSS/P3HT:PCBM/Al, with active-layer thickness varied between 100 and 400 nm. (b) Nanoscale morphology of the P3HT:PCBM bulk-heterojunction, showing donor-acceptor domains for exciton dissociation and charge transport

The thickness of the active layer was varied between 100 and 400 nm to study the balance between absorption and recombination. For a realistic description of charge generation and transport, the simulations used the P3HT:PCBM parameter set implemented in GPVDM (Table 2) [22], consistent with values reported in the literature [32, 33]. These parameters include carrier mobilities, trap densities, energetic disorder, dielectric constant, and optical constants. By explicitly adding trap-related properties, the model accounts for the recombination mechanisms that dominate in disordered organic solar cells (OSCs).

Table 2 – Electrical and optical parameters used in the P3HT:PCBM device simulations

Parameter	Value	Unit
Electron trap density	3.8×10^{26}	$m^{-3} \cdot eV^{-1}$
Hole trap density	1.45×10^{25}	$m^{-3} \cdot eV^{-1}$
Electron tail slope	40×10^{-3}	eV
Hole tail slope	60×10^{-3}	eV
Electron mobility (μ_e)	2.48×10^{-7}	$m^2 \cdot V^{-1} \cdot s^{-1}$
Hole mobility (μ_p)	2.48×10^{-7}	$m^2 \cdot V^{-1} \cdot s^{-1}$
Relative permittivity (ε_r)	3.8	–
Number of traps	20	–
Free electron → trapped electron rate	2.5×10^{-20}	m^{-2}
Trapped electron → free hole rate	1.32×10^{-22}	m^{-2}
Trapped hole → free electron rate	4.67×10^{-26}	m^{-2}
Free hole →trapped hole rate	4.86×10^{-22}	m^{-2}
Effective density of free electron states (N_e)	1.28×10^{27}	m^{-3}
Effective density of free hole states (N_p)	2.86×10^{25}	m^{-3}
Electron affinity (χ)	3.8	eV
Bandgap energy (E_g)	1.1	eV
n_free → p_free recombination rate constant	0	$m^3 \cdot s^{-1}$
Shunt resistance (R_{sh})	1.14	$\Omega \cdot m^2$
Series resistance (R_s)	19.5	Ω

This framework of structure and parameters makes it possible to systematically study how the active-layer thickness affects device performance under different illumination levels.

2.4 Limitations of the GPVDM Model

While GPVDM provides a flexible and accurate simulation framework, it's important to acknowledge several limitations:

- **Morphological averaging.** The model assumes a homogeneous active layer and therefore does not include nanoscale effects such as phase separation, domain purity, or interfacial sharpness. These factors, however, can strongly influence exciton dissociation and charge transport.
- **Simplified optics.** Light propagation is calculated using the transfer matrix method (TMM) with perfectly flat layers. This approach neglects scattering, surface roughness, and possible nanostructuring.
- **Parameter sensitivity.** Critical inputs such as the density of states, mobilities, and energy levels often differ between experiments and are not always simple to measure accurately. As a result, some mismatch between simulation and experiment can occur.

Even with these simplifications, GPVDM remains a dependable tool for predicting performance trends. It is particularly useful for analyzing thickness-illumination optimization in bulk-heterojunction OSCs, and its reliability is consistent with other simulation-based studies reported in the literature [34].

3. RESULTS AND DISCUSSION

Here, we look at how P3HT:PCBM organic solar cells perform under very different light levels. The range goes from weak indoor light (0.5-30 $W \cdot m^{-2}$) all the way up to strong outdoor sunlight (50-1100 $W \cdot m^{-2}$).

The study uses GPVDM simulations. We follow how the main parameters like short-circuit current (*J*sc), open-circuit voltage (*V*oc), fill factor (*FF*), and power conversion efficiency (PCE) change when both the active-layer thickness and the light intensity are varied.

The purpose is simple: to find thickness ranges that give the best efficiency for each lighting case. With this, one can suggest device designs that are better matched to real applications.

3.1 Impact of Illumination and Thickness on Electrical Output Parameters

The performance of organic solar cells depends on how well light is absorbed, how efficiently carriers are collected, and how much recombination occurs. Both the active-layer thickness and the incoming light intensity affect these processes in a strong way.

Short-circuit current density (*J*sc). Jsc rises with light intensity because a higher photon flux generates more excitons. Under outdoor sunlight, *J*sc can reach about 130 $A \cdot m^{-2}$ at 1100 $W \cdot m^{-2}$ for a 400 nm active layer. Indoors, under 30 $W \cdot m^{-2}$, the maximum is only 3.9 $A \cdot m^{-2}$. This difference of nearly two orders of magnitude comes not only from the lower photon flux indoors but also from the weaker spectral overlap between typical indoor light and the absorption of P3HT:PCBM.

The effect of thickness on *J*sc follows the Beer-Lambert law. At small thicknesses, making the active layer thicker increases the optical path and boosts absorption, so *J*sc rises almost linearly. At larger thicknesses, the growth slows down since most of the incoming light is already absorbed. Once the thickness goes beyond 400 nm, adding more material brings little benefit: carrier extraction becomes incomplete, and recombination losses dominate.

These results show the trade-off better absorption with thicker films, but reduced charge collection efficiency. The key point is that the optimal thickness depends on the illumination conditions.

Open-circuit voltage (*V*oc). Under outdoor illumination, Voc shows little dependence on active-layer thickness. This agrees with the Scharber model, which links Voc mainly to the donor-acceptor energy-level offset rather than to geometric factors. In this model, Voc is given by:

$$Voc = \frac{1}{q}\left(E_{HOMO_D} - E_{LUMO_A} - 0{,}3eV\right) \qquad (7)$$

where $E_{\mathrm{HOMO_D}}$ is the donor HOMO energy, $E_{\mathrm{LUMO_A}}$ is the

acceptor LUMO energy, and the empirical 0.3 eV term accounts for interfacial and recombination losses.

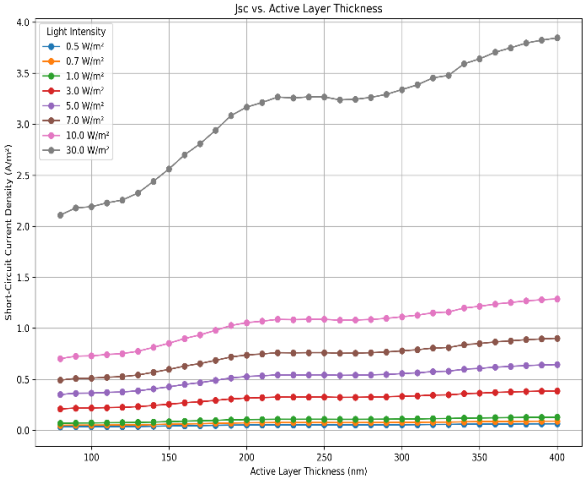


Fig. 4 – Short-circuit current density (*J*sc) of P3HT:PCBM solar cells as a function of active-layer thickness (100-400 nm) under indoor illumination intensities (0.5-30 W·m^{-2})

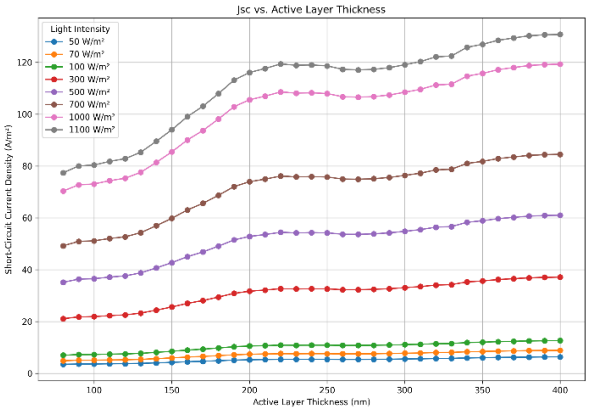


Fig. 5 – Short-circuit current density (*J*sc) of P3HT:PCBM solar cells as a function of active-layer thickness (100-400 nm) under outdoor illumination intensities (50-1100 W·m^{-2}).

In practice, *V*oc increases with light intensity, rising from 0.49 V at 50 W·m^{-2} to 0.61 V at 1100 W·m^{-2}. This behavior reflects the expected logarithmic dependence on carrier density. Under indoor light, the situation is very different: *V*oc falls sharply, reaching only 0.13 V at 1 W·m^{-2}. Here, the weak photogeneration limits the quasi-Fermi level splitting. At these low carrier densities, a small increase of Voc with thickness can be seen, which may suggest reduced recombination losses when the number of photogenerated charges is low.

Fill factor (*FF*). The fill factor is given by:

$$FF = \frac{V_{max} \, x \, J_{max}}{V_{oc} \, x \, J_{sc}} \tag{8}$$

where V_{max} and J_{max} are the voltage and current density at the maximum power point.

Under indoor illumination, *FF* increases with active-layer thickness up to around 200 nm and then tends to saturate. The initial rise can be linked to better charge collection and the reduction of interfacial resistance effects when the film is relatively thin. Beyond this thickness, however, adding more material brings little benefit, and *FF* reaches a plateau.

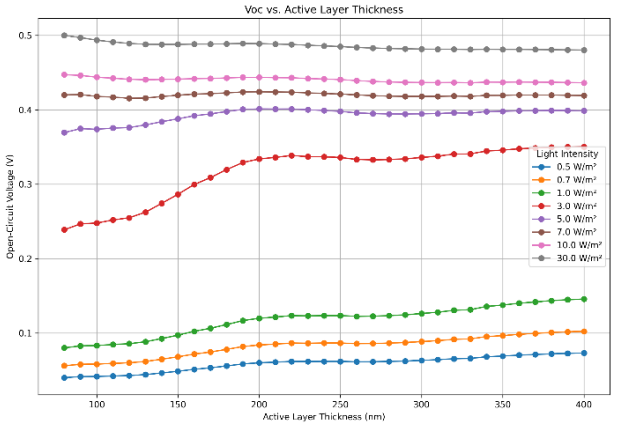


Fig. 6 – Open-circuit voltage (*V*oc) of P3HT:PCBM solar cells as a function of active-layer thickness (100-400 nm) under indoor illumination intensities (0.5-30 W·m^{-2})

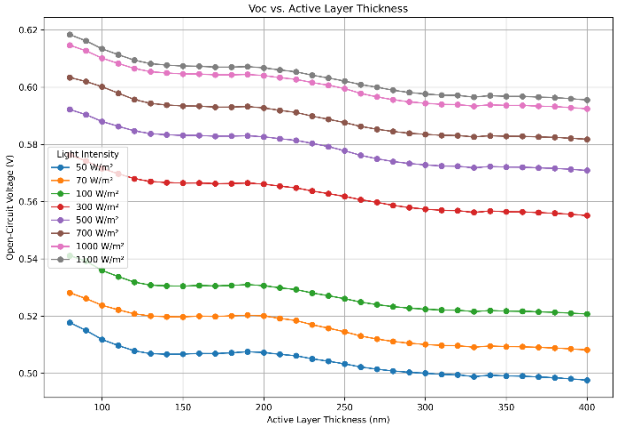


Fig. 7 – Open-circuit voltage (*V*oc) of P3HT:PCBM solar cells as a function of active-layer thickness (100-400 nm) under outdoor illumination intensities (50-1100 W·m^{-2})

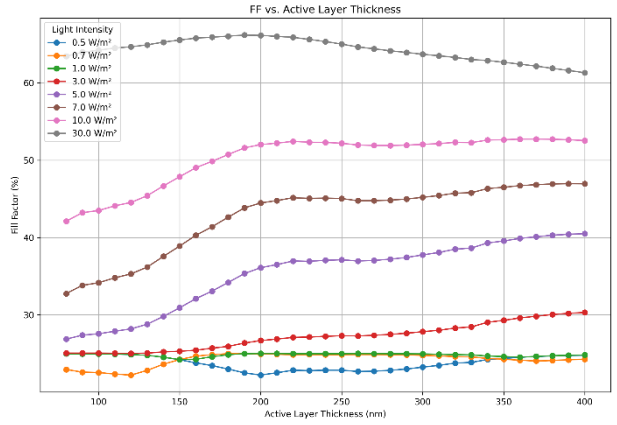


Fig. 8 – Fill factor (*FF*) of P3HT:PCBM solar cells as a function of active-layer thickness (100-400 nm) under indoor illumination intensities (0.5-30 W·m^{-2})

Outdoors, the situation is reversed. *FF* steadily decreases as the active layer becomes thicker. This drop is mainly due to stronger ohmic losses and more bulk recombination in thicker layers, which lower the charge extraction efficiency. The contrast between the indoor and outdoor cases highlights the need to balance absorption and transport losses when choosing the thickness of the active layer.

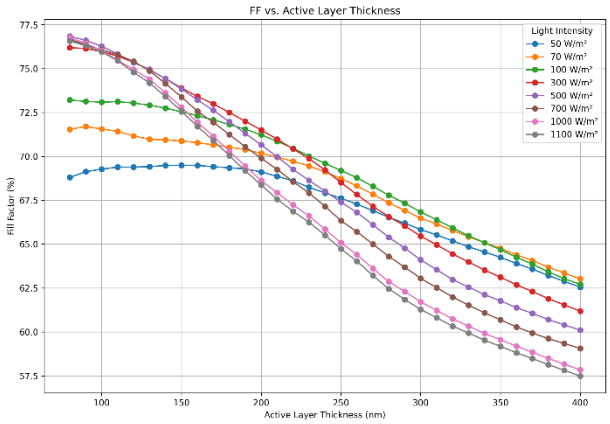


Fig. 9 – Fill factor (*FF*) of P3HT:PCBM solar cells as a function of active-layer thickness (100-400 nm) under outdoor illumination intensities (50-1100 W·m^{-2})

Power conversion efficiency (PCE). The power conversion efficiency is expressed as:

$$PCE = \frac{FF \times V_{oc} \times J_{sc}}{P_{light}} \quad (9)$$

where P_{light} is the incident illumination power density.

Under indoor illumination (0.5-30 W·m^{-2}), PCE increases with thickness and reaches a plateau between 200 and 240 nm. Still, the highest values are found closer to 350-400 nm, since absorption gains dominate at low irradiance. This behavior agrees with earlier reports showing that, under weak light, performance is mainly absorption-limited [35, 36].

Outdoors (50-1100 W·m^{-2}), the dependence on thickness is more complex. A first maximum appears around 200-220 nm, followed by a dip near 270-300 nm, and then a second plateau at 350-400 nm. The shift toward thinner optima under stronger illumination matches previous optimization studies on P3HT:PCBM and, more generally, polymer/fullerene BHJ systems [37, 38].

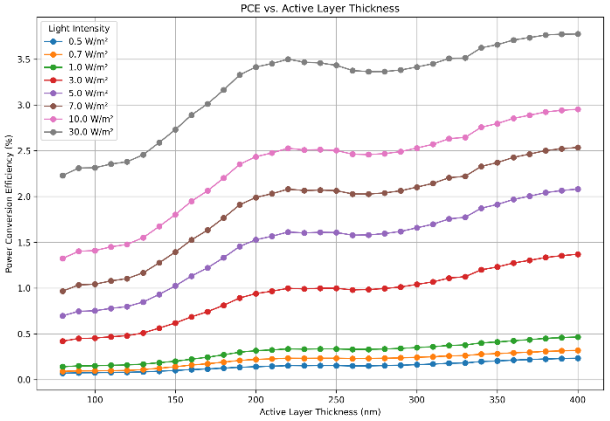


Fig. 10 – Power conversion efficiency (PCE) of P3HT:PCBM solar cells as a function of active-layer thickness (100-400 nm) under indoor illumination intensities (0.5-30 W·m^{-2})

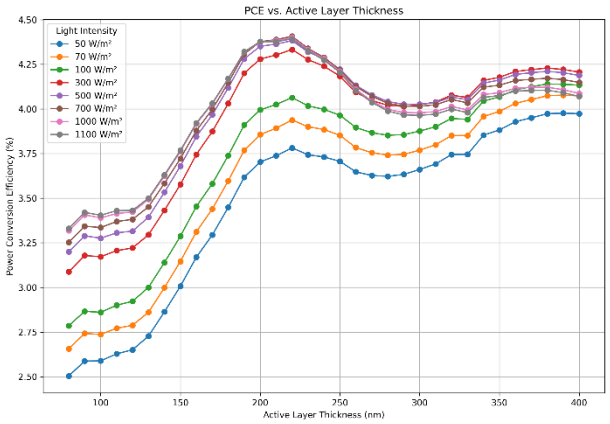


Fig. 11 – Power conversion efficiency (PCE) of P3HT:PCBM solar cells as a function of active-layer thickness (100-400 nm) under outdoor illumination intensities (50-1100 W·m^{-2})

Between 50 and 100 W·m^{-2}, thicker films (350-400 nm) still perform well, with efficiencies of about 3.9-4.1 %, since transport losses remain moderate. At higher intensities (> 300 W·m^{-2}), however, the best performance is obtained for thicknesses near 200-220 nm, where PCE reaches 4.4 %. Beyond this, efficiency saturates even though *J*sc keeps rising and *V*oc increases logarithmically. The main reason is a drop in *FF* at high photon flux, caused by stronger recombination [39, 40].

These results suggest a simple design rule: for indoor conditions, a thicker active layer improves absorption and boosts efficiency, while outdoors, thinner layers are favored to reduce transport losses and keep energy yields practical.

3.2 Application-Specific Thickness Recommendations

Based on the above analysis of photovoltaic parameters under different illumination levels, we suggest thickness ranges adapted to specific lighting environments. Aligning device geometry with realistic operating conditions maximizes efficiency and ensures the devices remain practical.

- **Ultra-low light (< 1 W·m^{-2}).** Even though the PCE stays below 0.5 %, OSCs can still power devices with very low consumption, such as intermittent sensors or passive IoT tags, where only a few microwatts are enough. In this regime, thickness plays little to no role.
- **Indoor low intensity (3-7 W·m^{-2}).** In typical office or commercial environments, thicker films over 300 nm reach efficiencies above 2.5 %. This amount is already sufficient for autonomous Bluetooth Low Energy (BLE) beacons, monitoring units, or other low-power electronics.
- **Indoor bright/semi-shaded outdoor (10-30 W·m^{-2}).** Layers in the range of 380–400 nm perform best here. They are suitable for applications such as smart windows, wearables, and building-integrated IoT systems.
- **Diffuse outdoor (50-150 W·m^{-2}).** In shaded locations or at high latitudes, films around 350-400 nm improve photon harvesting and provide stable efficiencies. This feature supports uses like environmental monitoring, city-scale IoT networks, and autonomous lighting.

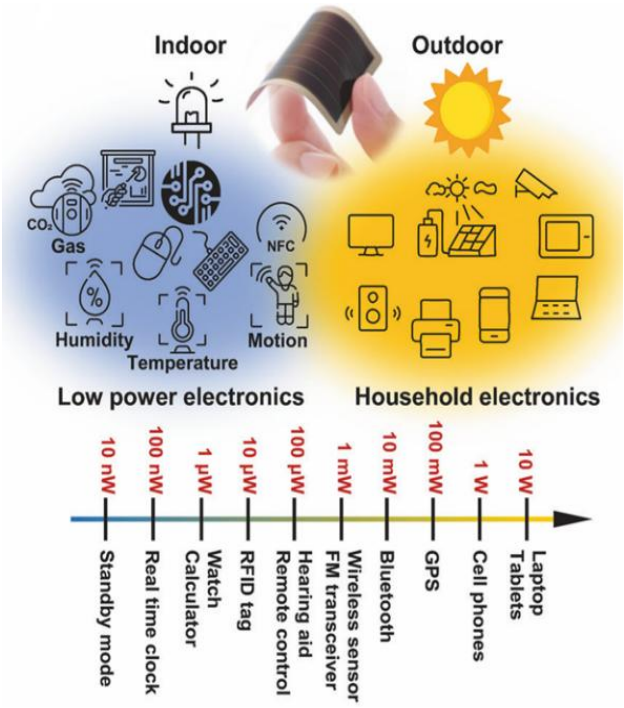


Fig. 12 – Representative indoor and outdoor applications of organic solar cells (OSCs) with typical power requirements, illustrating the link between illumination conditions and device operation [41]

- **Moderate outdoor (100-300 W·m⁻²).** A balanced thickness between 250 and 300 nm provides the best trade-off between absorption and transport. Such devices fit well with BIPV façades or outdoor wearable technologies.
- **High irradiance (300-700 W·m⁻²).** Thinner films of 220-250 nm help reduce recombination while keeping excellent absorption. These are a better choice for semi-portable IoT modules, compact PV tools, or outdoor harvesting devices.
- **Extreme irradiance (700-1100 W·m⁻²).** Very thin active layers, around 200-230 nm, are recommended. They minimize recombination losses under intense sunlight and allow robust operation in desert or tropical conditions. Typical examples include solar lanterns, USB charging units, or portable PV kits.

Figure 12 summarizes these results and links the suggested thickness ranges to different applications, from indoor electronics to outdoor energy-harvesting systems.

Following the application mapping in Figure 12, Table 3 formalizes the proposed design guidelines by linking illumination levels, optimal thickness ranges, and representative end-use scenarios.

The results in Table 3 show clearly that the best active-layer thickness depends strongly on the illumination regime. Under low or diffuse light, thicker films above 350 nm capture more photons and give higher efficiencies. Under strong sunlight, thinner layers around 200–250 nm perform better, since they limit recombination and cut resistive losses. This trade-off between absorption and transport is well known, and the agreement with experimental reports gives confidence in the reliability of the present simulations.

In summary, adjusting the thickness to the lighting environment allows an application-driven design of organic solar cells. The benefit is especially clear for indoor and low-light conditions. Beyond confirming the value of P3HT:PCBM as a model blend, these results show how simulation studies can provide practical guidelines for designing devices suited to real-world applications.

Table 3 – Optimal active-layer thickness recommendations for different illumination regimes and representative applications

Illumination (W/m²)	Optimal Thickness (nm)	Environment	Applications
< 1	Any (PCE < 0.5 %)	Ultra-low indoor (LED signage, dim light)	Intermittent sensors, passive IoT tags
3-7	> 300	Indoor (offices, commercial spaces)	BLE beacons, monitoring electronics
10-30	380-400	Bright indoor / semi-shaded outdoor	Smart windows, wearables, indoor IoT
50-150	350-400	Diffuse outdoor (forests, high latitudes)	Environmental monitoring, urban IoT, autonomous lighting
100-300	250-300	Moderate outdoor (temperate climates, urban areas)	BIPV façades, outdoor wearables
300-700	220-250	High-irradiance outdoor (Mediterranean, California)	Semi-portable IoT modules, compact PV tools
700-1100	200-230	Extreme irradiance (deserts, tropics)	Solar lanterns, USB chargers, portable PV kits

4. CONCLUSION

Optimizing organic solar cells according to the illumination conditions they will face is a useful way to improve efficiency and enhance their practical relevance. In this work we used GPVDM to simulate P3HT:PCBM bulk-heterojunction devices under light intensities from 0.5 to 1100 W·m⁻², paying close attention to the role of active-layer thickness.

The results make it clear that performance is very sensitive to both illumination and thickness. Indoors or under weak light, thicker films (350-400 nm) absorb more and can reach about 3.75 % efficiency. That is enough to run small devices like IoT sensors, BLE beacons, or printed circuits. Outside, in full sun, thinner layers around 220 nm present the best compromise between absorption and transport. This agrees with what experiments usually show and fits applications such as BIPV façades or portable PV modules.

In the end, the study suggests a simple design rule:

match the thickness of the active layer to the environment. Doing so turns a basic material like P3HT:PCBM into a clear example of how simulations can lead to practical guidelines. The same method can also be applied to newer materials, including non-fullerene blends. Therefore, the approach is flexible, and it can support the development of the next generation of organic photovoltaics.

REFERENCES

1. International Energy Agency, *Renewables 2023: Analysis and Forecasts to 2028* (Paris: IEA, 2024).
2. R. García-Valverde, J.A. Cherni, A. Urbina, *Prog. Photovolt.: Res. Appl.* **18**, 535 (2010) https://doi.org/10.1002/pip.967.
3. A.L. Roes, E.A. Alsema, K. Blok, M.K. Patel, *Prog. Photovolt.: Res. Appl.* **17**, 372 (2009) https://doi.org/10.1002/pip.891.
4. Y. Cui, L. Hong, T. Zhang, H. Meng, H. Yan, F. Gao, J. Hou, *Joule* **5**, 1011 (2021) https://doi.org/10.1016/j.joule.2021.03.029.
5. L. Duan, A. Uddin, *Adv. Sci.* **7**, 1903259 (2020) https://doi.org/10.1002/advs.201903259.
6. E.K. Solak, E. Irmak, *RSC Adv.* **13**, 12244 (2023) https://doi.org/10.1039/D3RA01454A.
7. M.C. Scharber, D. Mühlbacher, M. Koppe, P. Denk, C. Waldauf, A.J. Heeger, C.J. Brabec, *Adv. Mater.* **18**, 789 (2006) https://doi.org/10.1002/adma.200501717.
8. Fraunhofer Institute for Solar Energy Systems ISE, *Photovoltaics Report* (Freiburg: Fraunhofer ISE: 2024).
9. Research Nester, *Organic Solar Cells Market Size & Share – Forecast Report 2025–2037*, Report ID 3513 (2025) https://www.researchnester.com/reports/organic-pv-solar-cells-market/3513.
10. C. Chen, L. Wang, W. Xia, K. Qiu, C. Guo, Z. Gan, J. Zhou, Y. Sun, D. Liu, W. Li, T. Wang, *Nat. Commun.* **15**, 6865 (2024) https://doi.org/10.1038/s41467-024-51359-w.
11. K. Liu, Y. Jiang, G. Ran, F. Liu, W. Zhang, X. Zhu, *Joule* **8**, 835 (2024) https://doi.org/10.1016/j.joule.2024.01.005.
12. J. Wang, Z. Zheng, P. Bi, Z. Chen, Y. Wang, X. Liu, S. Zhang, X. Hao, M. Zhang, Y. Li, J. Hou, *Natl. Sci. Rev.* **10**, nwad085 (2023) https://doi.org/10.1093/nsr/nwad085.
13. J. Wang, J. Li, Y. Wang, J. Ren, P. Bi, H. Li, J. Dai, S. Zhang, J. Hou, *Adv. Mater.* **37**, e10378 (2025) https://doi.org/10.1002/adma.202510378.
14. H.K.H. Lee, J. Wu, J. Barbé, S.M. Jain, S. Wood, E.M. Speller, Z. Li, F.A. Castro, J.R. Durrant, W.C. Tsoi, *J. Mater. Chem. A* **6**, 5618 (2018) https://doi.org/10.1039/C7TA10875C.
15. A. Chakraborty, G. Lucarelli, J. Xu, Z. Skafi, S. Castro-Hermosa, A.B. Kaveramma, R.G. Balakrishna, T.M. Brown, *Nano Energy* **128**, 109932 (2024) https://doi.org/10.1016/j.nanoen.2024.109932.
16. World Bank Group, Solargis, *Global Solar Atlas 2.12* (2024) https://globalsolaratlas.info.
17. D. Lübke, P. Hartnagel, M. Hülsbeck, T. Kirchartz, *ACS Mater. Au* **3**, 215 (2023) https://doi.org/10.1021/acsmaterialsau.2c00070.
18. O. Ourahmoun, *J. Nano-Electron. Phys.* **11** No 2, 02004 (2019) https://doi.org/10.21272/jnep.11(2).02004.
19. A.S. Alali, M. Oduncuoglu, F. Touati, *Nanomaterials* **14**, 1146 (2024) https://doi.org/10.3390/nano14131146.
20. S. Wilken, D. Scheunemann, S. Dahlström, M. Nyman, J. Parisi, R. Österbacka, *Adv. Electron. Mater.* **7**, 2001056 (2021) https://doi.org/10.1002/aelm.202001056.
21. A.K. Mishra, R.K. Shukla, *Mater. Today: Proc.* **49**, 321 (2021) https://doi.org/10.1016/j.matpr.2020.11.376.
22. R.C.I. MacKenzie, *OghmaNano – Organic and Hybrid Material Nano Simulation Tool*, https://www.oghma-nano.com (accessed 13 June 2026).
23. N. Chandrasekaran, A. Kumar, L. Thomsen, D. Kabra, C.R. McNeill, *Mater. Adv.* **2**, 2045 (2021) https://doi.org/10.1039/D0MA00738B.
24. O. Oklobia, T.S. Shafai, *Sol. Energy Mater. Sol. C.* **122**, 158 (2014) https://doi.org/10.1016/j.solmat.2013.11.035.
25. M.K. Omrani, H. Fallah, K.-L. Choy, M. Abdi-Jalebi, *Sci. Rep.* **11**, 19774 (2021) https://doi.org/10.1038/s41598-021-99095-1.
26. M.N. Zidan, N. Everitt, T. Ismail, I.S. Fahim, *Polymers* **13**, 3224 (2021) https://doi.org/10.3390/polym13193224.
27. G. Grancharov, M.-D. Atanasova, R. Kalinova, R. Gergova, G. Popkirov, C. Dikov, M. Sendova-Vassileva, *Molecules* **26**, 6890 (2021) https://doi.org/10.3390/molecules26226890.
28. A.Y. Ali, N.P. Holmes, N. Cooling, J. Holdsworth, W. Belcher, P. Dastoor, X. Zhou, *Coatings* **13**, 1293 (2023) https://doi.org/10.3390/coatings13071293.
29. B. Balraj, M. Raja, T.G. Vignesh Prabhu, M. Balaji, J. Chandrasekaran, S.K. Nagarajan, M. Bharathi, S. Lee, C. Sivakumar, *Sol. Energy* **297**, 113574 (2025) https://doi.org/10.1016/j.solener.2025.113574.
30. M.T. Dang, L. Hirsch, G. Wantz, *Adv. Mater.* **23**, 3597 (2011) https://doi.org/10.1002/adma.201100792.
31. O.J.J. Ronsin, J. Harting, *ACS Appl. Mater. Interfaces* **14**, 49785 (2022) https://doi.org/10.1021/acsami.2c14319.
32. Y. Kim, S. Cook, S.M. Tuladhar, S.A. Choulis, J. Nelson, J.R. Durrant, D.D.C. Bradley, M. Giles, I. McCulloch, C.-S. Ha, M. Ree, *Nat. Mater.* **5**, 197 (2006) https://doi.org/10.1038/nmat1574.
33. A. Ng, X. Liu, C.H. To, A.B. Djurišić, J.A. Zapien, W.K. Chan, *ACS Appl. Mater. Interfaces* **5**, 4247 (2013) https://doi.org/10.1021/am4004232.
34. B. Farhadi, F. Zabihi, Y. Zhou, A. Liu, *J. Nano-Electron. Phys.* **13** No 1, 01007 (2021) https://doi.org/10.21272/jnep.13(1).01007.
35. S. Biswas, Y. Lee, H. Choi, H.W. Lee, H. Kim, *RSC Adv.* **13**, 32000 (2023) https://doi.org/10.1039/D3RA02599C.
36. H.S. Ryu, S.Y. Park, T.H. Lee, J.Y. Kim, H.Y. Woo, *Nanoscale* **12**, 5792 (2020) https://doi.org/10.1039/D0NR00816H.
37. M. Shaban, M. Benghanem, A. Almohammedi, M. Rabia, *Coatings* **11**, 863 (2021) https://doi.org/10.3390/coatings11070863.
38. J. Vlahović, M. Stanojević, J. Gojanović, J. Melancon, A. Sharma, S. Živanović, *Opt. Exp.* **29**, 8710 (2021) https://doi.org/10.1364/OE.418082.
39. S. Ryu, N.Y. Ha, Y.H. Ahn, J.-Y. Park, S. Lee, *Sci. Rep.* **11**, 16781 (2021) https://doi.org/10.1038/s41598-021-96222-w.
40. B. Xiao, P. Calado, R.C.I. MacKenzie, T. Kirchartz, J. Yan, J. Nelson, *Phys. Rev. Appl.* **14**, 024034 (2020) https://doi.org/10.1103/PhysRevApplied.14.024034.
41. S. Hwang, T. Yasuda, *Polym. J.* **55**, 297 (2023) https://doi.org/10.1038/s41428-022-00727-8.

Оптимізація товщини органічних сонячних елементів для конкретних умов застосування: у приміщенні та на відкритому повітрі

W. Guanoune[1], H.A. Abbassi[2]

[1] *Badji Mokhtar University, Faculty of Sciences, Department of Physics, 23000 Annaba, Algeria*
[2] *Environmental Research Center (CRE), Environmental Innovation and Eco-Waste Management Division, 23000 Annaba, Algeria*

Органічні сонячні елементи (ОСЕ) вирізняються гнучкістю та низькою вартістю виготовлення, проте їхня ефективність суттєво залежить від умов освітлення. Стандартна оптимізація за умов AM1.5G (1000 Вт·м$^{-2}$) не враховує різноманіття реальних умов експлуатації – від слабкого освітлення в приміщеннях (менше 1 Вт·м$^{-2}$) до інтенсивного сонячного світла. У цій роботі ми розробили рекомендації щодо вибору товщини активного шару залежно від рівня освітленості, пов'язуючи геометрію пристрою з конкретними сферами його застосування. За допомогою програмного забезпечення OghmaNano (GPVDM) було проведено моделювання процесів дрейфу та дифузії в сонячних елементах із об'ємним гетеропереходом на основі суміші P3HT:PCBM за інтенсивності світла від 0,5 до 1100 Вт·м$^{-2}$. Результати показали, що в умовах приміщення (1-30 Вт·м$^{-2}$) використання товстіших активних шарів (350-400 нм) дозволяє максимізувати поглинання світла та досягти ефективності перетворення енергії (PCE) до 3,75 %. Натомість за умов високої зовнішньої освітленості (≥ 700 Вт·м$^{-2}$) тонші шари (200-230 нм) сприяють зменшенню рекомбінації носіїв заряду та підвищують вихідну потужність. Розроблена карта проектування, що пов'язує параметри PCE, *Jsc*, *Voc* та *FF* із поєднанням товщини шару й інтенсивності світла, дозволяє визначити оптимальні характеристики для конкретних умов експлуатації. Хоча методологію було продемонстровано на прикладі системи P3HT:PCBM, вона є універсальною і може застосовуватися до інших технологій органічної фотовольтаїки. Отримані результати надають чіткі рекомендації щодо вибору товщини шару з урахуванням умов освітлення, що дозволяє ефективно перенести результати лабораторної оптимізації на реальні умови експлуатації ОСЕ – як у приміщеннях, так і на відкритому повітрі.

Ключові слова: Органічні сонячні елементи, Товщина активного шару, Дрейфово-дифузійне моделювання, Залежність від інтенсивності світла, Фотовольтаїка для приміщень.